Sensorless Speed Measurement of AC Machines Using Analytic Wavelet Transform

José M. Aller, Thomas G. Habetler, *Fellow, IEEE*, Ronald G. Harley, *Fellow, IEEE*, Rangarajan M. Tallam, *Member, IEEE*, and Sang Bin Lee, *Member, IEEE*

***Abstract*—A new method for sensorless speed estimation of ac machines, using the analytic wavelet transform of the stator current signal, is proposed for a direct torque control drive. A comparison with results obtained using the short-time Fourier transform is included. The proposed method can be implemented in real time on a digital signal processor. The time–frequency resolution obtained and the computation time required by the proposed algorithm are improved in comparison to existing techniques, and the method can be applied over the entire speed range.**

***Index Terms*—AC machines, analytic wavelet transform, direct torque control, sensorless speed estimation, short-time Fourier transform.**

I. Introduction

ADVANCES in power semiconductor device technology have led to the widespread use of ac drives using advanced control techniques such as field-oriented control or direct torque control (DTC). However, in spite of the robustness of variable-speed ac drives, the requirement of a shaft-mounted speed sensor renders them less attractive.

Estimators, observers, and spectral analysis methods [1]–[4] are the frequently used techniques for sensorless speed estimation. The performance of speed estimators depends on the accuracy of the machine model and parameter estimator. Observers for speed estimation have a relatively long delay time that can limit speed detection during a transient. The resolution obtained with spectral analysis is restricted by the uncertainty principle represented by the Heisenberg boxes [5], shown in Fig. 1. Ridges algorithms [5], [6] can solve this problem efficiently.

Paper IPCSD 02–019, presented at the 2001 IEEE Applied Power Electronics Conference and Exposition, Anaheim, Ca, March 4–8, and approved for publication in the IEEE TRANSACTIONS ON INDUSTRY APPLICATIONS by the Industrial Drives Committee of the IEEE Industry Applications Society. Manuscript submitted for review December 11, 2000 and released for publication May 15, 2002.

J. M. Aller is with the Departamento de Conversión y Transporte de Energía, Universidad Simón Bolívar, Caracas 1080-A, Venezuela (e-mail: jaller@usb.ve).

T. G. Habetler and R. G. Harley are with the School of Electrical and Computer Engineering, Georgia Institute of Technology, Atlanta, GA 30332 USA (e-mail: tom.habetler@ece.gatech.edu; ron.harley@ece.gatech.edu).

R. M. Tallam was with the School of Electrical and Computer Engineering, Georgia Institute of Technology, Atlanta, GA 30332 USA. He is now with the Advanced Technology Laboratories, Rockwell Automation, Milwaukee, WI 53201 USA (e-mail: rmtallam@ra.rockwell.com).

S. B. Lee was with the School of Electrical and Computer Engineering, Georgia Institute of Technology, Atlanta, GA 30332 USA. He is now with the Electromechanical Energy Conversion Laboratory, General Electric Corporate Research and Development, Niskayuna, NY 12309 USA (e-mail: sang.lee@crd.ge.com).

Publisher Item Identifier 10.1109/TIA.2002.802988.

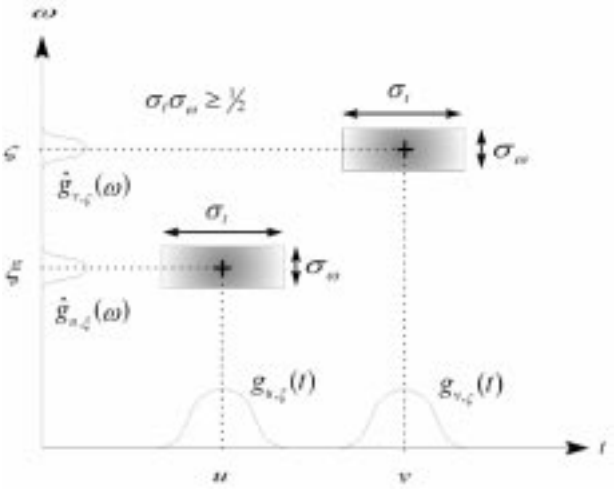

Fig. 1. Heisenberg boxes for STFT using the window $g(t)$.

The short-time Fourier transform (STFT) is a practical tool to measure the frequency variations in time. The time–frequency information is contained in plane boxes called atoms, defined by the spread in time and frequency that contain enough energy density to be useful in signal processing. When a classical window is employed (Gaussian, Hanning, Hamming, etc.), the information is spread over a rectangular atom in the time–frequency plane; this atom area is minimum when a Gaussian window is used. In the STFT, the atom rectangle is the same at all time instants for every window (Fig. 1).

The instantaneous frequency can be obtained from ridge analysis, thereby increasing the time–frequency resolution of the Heisenberg boxes. This method has been widely applied in sensorless speed estimations of ac machines [2]–[4].

Wavelet analysis is a more general transformation and is also based on internal products of functions. However, in this case the concept of scale replaces the frequency variable of the Fourier transform. Although the Heisenberg atom area is not smaller than in the STFT with a Gaussian window, the time or frequency resolution can be conveniently changed using different scales, increasing one variable and decreasing the other (equal area atoms). This idea is illustrated in Fig. 2.

This additional degree of freedom can improve the angular speed resolution (including the low-speed range), in transient or steady-state operation. The instantaneous frequency information can be obtained using a few scales appropriately chosen with a base 2 logarithmic distribution, $s^{-1} = \{2, 4, 8, \ldots, 2^m\}$. The ridge algorithm can also be

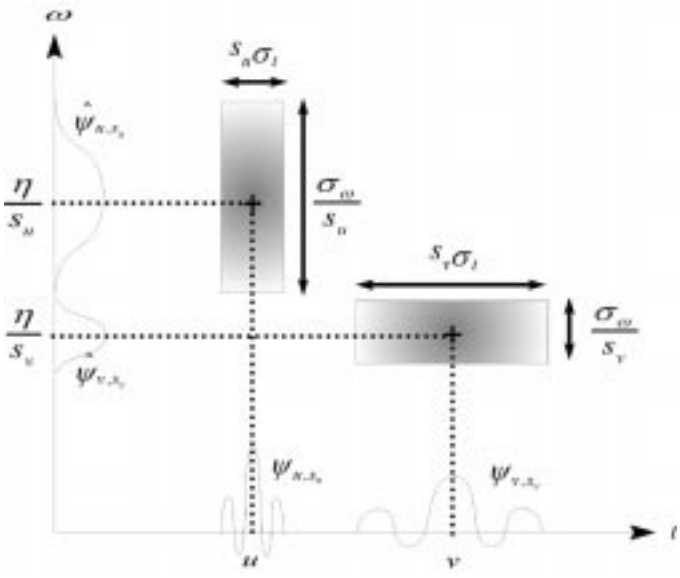

Fig. 2. Heisenberg boxes for analytic wavelet transform using two different scales.

applied in this case to obtain the instantaneous frequency, as with the STFT, to increase the time–frequency resolution [6].

In this paper, the stator current of an induction machine with a DTC drive [7]–[10], is analyzed using the analytic wavelet transform (AWT) and the STFT. The results obtained are compared with the angular speed measured with a high-resolution optical encoder.

Wavelet analysis has been applied to reduce torque ripple in DTC drives [11]. Using the same coefficients obtained in this application, the proposed technique can be extended to obtain the angular speed, with just the additional use of the ridges algorithm.

II. Time-Frequency Analysis

A. Short-Time Fourier Transform

The frequency content of the stator current spectrum as a function of time can be analyzed using the STFT, also called windowed Fourier transform (WFT). In the STFT, a Gabor atom, $g_{u,\xi}(t)$, is used to measure the frequency variations in a time signal [2], [4], [5]. A family of time–frequency Gabor atoms is obtained by modulating the real and symmetric function (window), $g(t)$, by the frequency ξ and translating it by the center time u

$$g_{u,\xi}(t) = e^{j\xi t} g(t-u). \tag{1}$$

The STFT of the function $f(t)$ at a particular time u, and frequency ξ is

$$Sf(u,\xi) = \langle f, g_{u,\xi}\rangle = \int_{-\infty}^{+\infty} f(t) e^{j\xi t} g(t-u)\, dt. \tag{2}$$

The spectrogram of the function $f(t)$ is the energy density of this signal and can be defined as

$$P_S f(u,\xi) = |Sf(u,\xi)|^2. \tag{3}$$

The spectrogram can be represented in a three-dimensional (3-D) plot and its ridges represent the instantaneous frequency $\omega(t)$ [5]

$$\omega(t) = \frac{d}{dt}\phi(t) \geq 0 \tag{4}$$

where

$$f(t) = a(t)\cos\phi(t), \qquad \text{with } a(t) > 0.$$

The resolution in time and frequency of the STFT depends on the spread in time and frequency of the selected window (Rectangle, Hamming, Gaussian, Hanning, etc.). This area is minimum (1/2) when the Gaussian window is used [5].

B. AWT

To analyze the frequency content of the stator current spectrum as a function of time using the wavelet transformation, it is necessary to use an analytic wavelet$\psi(t)$ [5]. A family of time–frequency wavelet atoms is obtained by scaling the wavelet function ψ by the scale s and translating it by the center time u

$$\psi_{u,s}(t) = \frac{1}{\sqrt{s}}\,\psi\left(\frac{t-u}{s}\right). \tag{5}$$

The wavelet transform of $f(t)$ at a particular time u and scale s is

$$Wf(u,s) = \langle f, \psi_{u,s}\rangle = \int_{-\infty}^{+\infty} f(t)\frac{1}{\sqrt{s}}\,\psi^*\left(\frac{t-u}{s}\right) dt. \tag{6}$$

The Fourier–Parseval formula can be used to calculate the wavelet transform using the frequency information

$$Wf(u,s) = \int_{-\infty}^{+\infty} f(t)\psi^*_{u,s}(t)\, dt = \frac{1}{2\pi}\int_{-\infty}^{+\infty} \hat{f}(\omega)\hat{\psi}^*_{u,s}(\omega)\, d\omega. \tag{7}$$

An analytic wavelet can be constructed by modulating the frequency ($e^{j\eta t}$) of a real and symmetric window $g(t)$. A Gabor wavelet $\psi(t) = g(t)e^{j\eta t}$ is obtained from a Gaussian window

$$g(t) = (\sigma^2\pi)^{-(1/4)}\exp\left(\frac{-t^2}{2\sigma^2}\right). \tag{8}$$

If $\sigma^2\eta^2 \gg 1$, then $\hat{g}(\omega) \approx 0$ for $|\omega| > \eta$, and the wavelet function can be considered approximately analytic. The Fourier transform of the Gaussian window (8) is

$$\hat{g}(\omega) = (4\pi\sigma^2)^{1/4}\exp\left(-\frac{\sigma^2\omega^2}{2}\right). \tag{9}$$

The Fourier transform of the Gabor wavelet is

$$\hat{\psi}(\omega) = \hat{g}(\omega-\eta). \tag{10}$$

The Fourier transform of $\psi_{u,s}$ is a dilation of $\hat{\psi}(\omega)$ by $1/s$, and can be obtained as

$$\hat{\psi}_{u,s}(\omega) = \sqrt{s}\,\hat{\psi}(s\omega)\exp(-j\omega u). \tag{11}$$

The inverse Fourier transform of the frequency function obtained by multiplying $\hat{f}(\omega)$ with $\sqrt{s}\,\hat{\psi}(s\omega)$ is directly the AWT

$Wf(u, s)$. Equations (7) and (11) give a simple and fast method to obtain the AWT using the classic fast Fourier transform (FFT) algorithm. If an analytic wavelet function is chosen, its Fourier transform is known; hence, computational complexity can be reduced by using the FFT to obtain the Fourier transform of $f(t)$ and the inverse Fourier transform for each scale, s, under analysis. The number of required scales depends on the frequency spectrum being analyzed.

An analytic wavelet transform defines a local time–frequency energy density

$$P_W f(u, s) = |Wf(u, s)|^2. \tag{12}$$

This energy density is called a scalogram and can be represented on a three-dimensional plot. The instantaneous frequency $\xi(t)$ can be obtained directly from the ridge algorithm defined over the scalogram [6]. The instantaneous frequency $\xi(t)$ is related to the ridges of the normalized scalogram $s^{-1}P_W f(u, s)$ as

$$\xi(u) = \eta/s(u). \tag{13}$$

The scalogram defined in (12) is linear in the time axis, but logarithmic (base 2) in the scale axis. To obtain a linear frequency spectrogram, similar to (3), logarithmic interpolation and application of (13) are required.

C. Ridges Algorithm

The instantaneous frequency defined in (4) can be estimated by ridges detection in the spectrogram. The spectrogram can be obtained using any time–frequency transform such as: STFT, AWT or Wigner–Ville. However, the signal $f(t)$ can contain several spectral lines. In this case some additional considerations are necessaries for frequency discrimination. Suppose that the signal is composed of several frequency components

$$f(t) = \sum a_k(t) \cos \phi_k(t) \tag{14}$$

where $a_k(t)$ and $\phi'_k(t)$ have small variations over the intervals of size s and $s\phi'_k(t) \geq \Delta\omega$. Each instantaneous component can be discriminated by the STFT if the frequency difference is larger than the bandwidth of the Fourier transform of the Gaussian window $\hat{g}(s\omega)$ [5], [6]

$$\left|\phi'_i(u) - \phi'_j(u)\right| \geq \frac{\Delta\omega}{s}. \tag{15}$$

If AWT is applied, instantaneous frequencies can be discriminated when the following bandwidth relation is satisfied [5]:

$$\frac{\left|\phi'_i(u) - \phi'_j(u)\right|}{\phi'_i(u)} \geq \frac{\Delta\omega}{\eta} \quad \text{and} \quad \frac{\left|\phi'_i(u) - \phi'_j(u)\right|}{\phi'_j(u)} \geq \frac{\Delta\omega}{\eta}. \tag{16}$$

Relations (15) and (16) are useful tools for selecting scales and bandwidth for the wavelet and Gabor functions.

The ridge algorithm determines instantaneous frequencies from local maxima on the spectrogram $P_S f(u, \xi)$. For this reason, the scalogram must be linearized in the wavelet analysis.

III. Experimental Results

A DTC system was developed using a commercial digital signal processor (DSP) platform (based on TMS320C44 floating-point DSP − max. 60 MFLOPS) that includes four 16-bit A/D converters (200 kHz per channel) and 32 bits of digital I/O. The DSP was programmed to obtain line-to-line voltages, and line currents of an inverter-fed 5.0-hp 208-V 1760-r/min 60-Hz squirrel-cage motor. Inverter transistors are activated by six digital outputs generated by the DSP. The sampling frequency was chosen to be 10 kHz. Data acquisition and generation of insulated gate bipolar transistor (IGBT) gate drives for the DTC scheme are performed during the 100-μs window. The electromagnetic torque and the stator flux are defined as references. These variables are estimated using the instantaneous voltages and currents measured at the machine terminals. The stator line-to-line voltages are estimated by measuring the dc-bus voltage and the inverter switching state at any instant. The stator flux vector is obtained by integrating the terminal voltage

$$\vec{\lambda}_s = \int_o^t \vec{e}_s \, dt = \int_o^t \left(\vec{v}_s - R_s \vec{i}_s\right) dt \tag{17}$$

where

$$\vec{v}_s \equiv \frac{\sqrt{2}}{3} e^{-j(\pi/6)} \left(v_{ab} + v_{bc} e^{j(2\pi/3)} + v_{ca} e^{j(4/3)}\right)$$

$$\vec{i}_s \equiv \sqrt{\frac{2}{3}} \left(i_a + i_b e^{j(2\pi/3)} + i_c e^{j(4\pi/3)}\right).$$

The torque is estimated directly as

$$T_e = \vec{\lambda}_s \times \vec{i}_s. \tag{18}$$

Errors between reference and estimated values of torque and flux are used to switch the inverter devices according to the classical DTC scheme [7]–[10].

Fig. 3 shows a block diagram of the experimental system. The PC monitor loads the control program into the DSP platform, and reads the instantaneous measured variables of the induction motor using the A/D converters. The DSP drives the inverter transistors, acquires and digitizes ac currents and the dc voltage. Encoder information is read by the DSP using a digital I/O port. The direct memory access (DMA) port is used to communicate with the DSP and PC monitor.

Fig. 4 shows the speed observer algorithm using the spectrogram or scalogram method. The speed observer actually runs in the PC monitor, but can also be implemented in the DSP to perform online speed estimation.

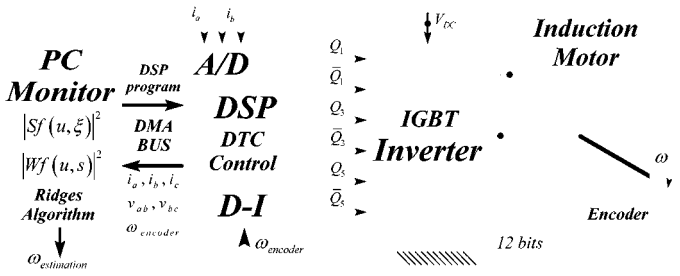

Fig. 3. Block diagram of the experimental system.

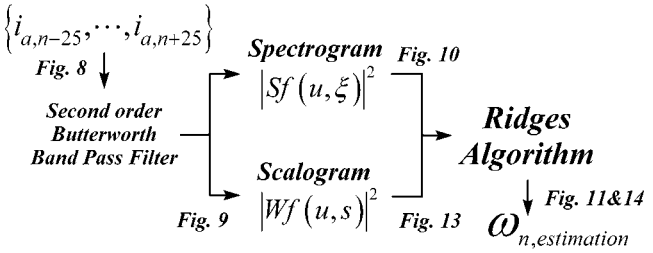

Fig. 4. Speed observer algorithm.

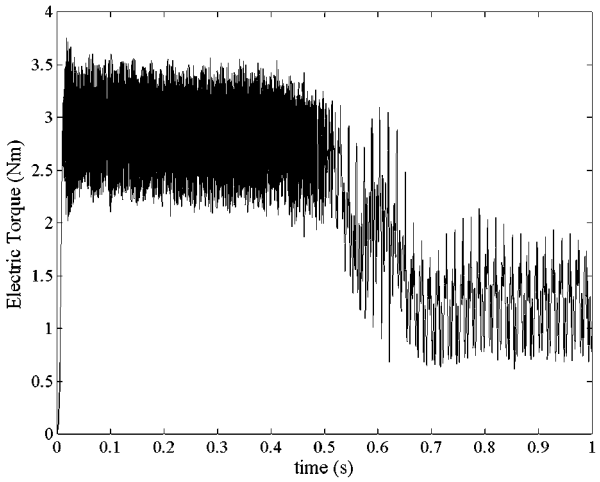

Fig. 5. Instantaneous electromagnetic torque during startup with a DTC drive (constant torque and flux references).

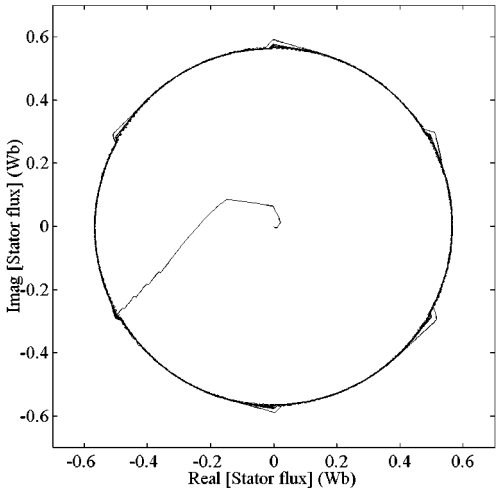

Fig. 6. Space vector of the stator flux during startup with a DTC drive (constant torque and flux references).

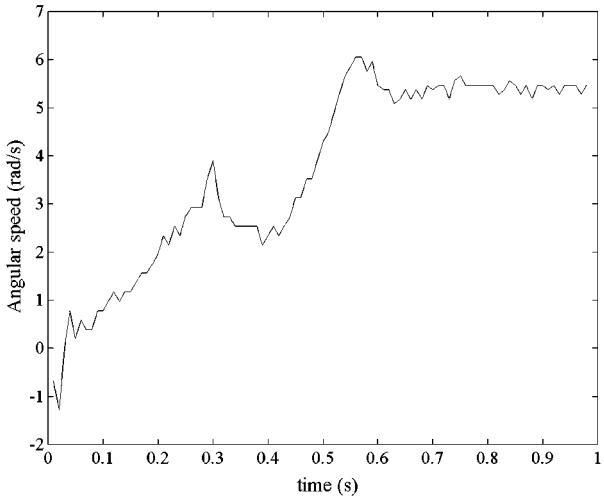

Fig. 7. Angular speed of the induction machine during startup measured with an optical encoder.

The squirrel-cage motor is started without load, using 3.0 N·m as the reference torque and 0.6 Wb as the flux reference. After the acceleration process, the torque is not maintained at its reference value; the DTC algorithm can only adjust the stator flux when the final speed is reached. Fig. 5 shows the electric torque during the no-load startup of the induction motor at constant torque and flux ($0.0 \leq t \leq 1.0$ s). Fig. 6 shows the space-vector diagram of the stator flux under the same condition.

An optical incremental encoder with 1024 ppt is coupled to the motor shaft to perform a direct measure of the angular speed. The DTC algorithm reads the incremental count each 10 ms and calculates the speed. Fig. 7 shows that the angular speed obtained by the encoder. Observe that the speed increase is not linear, even though the average torque during this time is constant. This is due to the nonlinearity of the mechanical load in the low speed range (static and dynamic friction).

Fig. 8 shows the current in one phase during the startup. The stator current has some harmonic components related to the inverter operation (variable-frequency commutation), and others given by the slot harmonics.

A digital second-order Butterworth bandpass filter (50–500 Hz) is used to preprocess the stator current signal. In this way, some interference frequencies coming from the inverter as well as the fundamental component are eliminated. The filtered signal is shown in Fig. 9.

The filtered signal in Fig. 9 has information about the slot harmonics and hence, angular speed. The spectrogram $P_S f(u, \xi)$ shown in Fig. 10 is obtained using a Gaussian window with 50 points. Darker zones in Fig. 10 represent high values of the spectrogram function and could be represented by a 3-D plot. Fig. 11 shows the instantaneous frequencies after the use of the ridges algorithm and contains areas of no information, or breaks in the curves. This is due to interference from the inverter produced harmonics. Fig. 12 contains the details of the spectrogram at the time instant $t = 0.5$ s, to illustrate the ridges detection in Fig. 11.

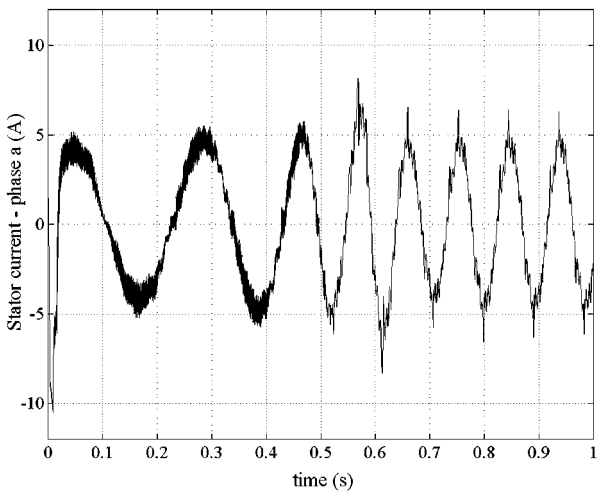

Fig. 8. Stator current of the induction machine during a DTC startup with constant torque and flux references.

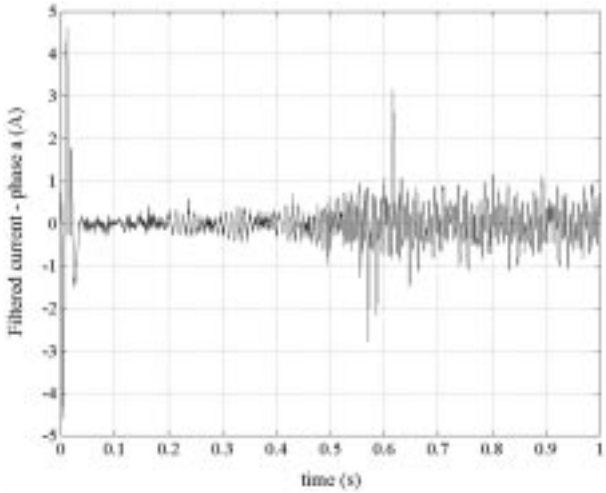

Fig. 9. Stator current processed by the second-order Butterworth bandpass filter.

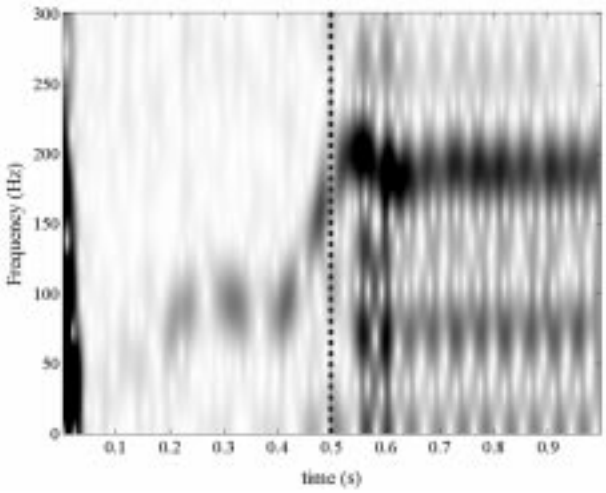

Fig. 10. STFT spectrogram of the filtered current obtained using a Gaussian window with 50 points.

It is clear that the use of the ridges algorithm improves the frequency resolution from Fig. 10 to 11.

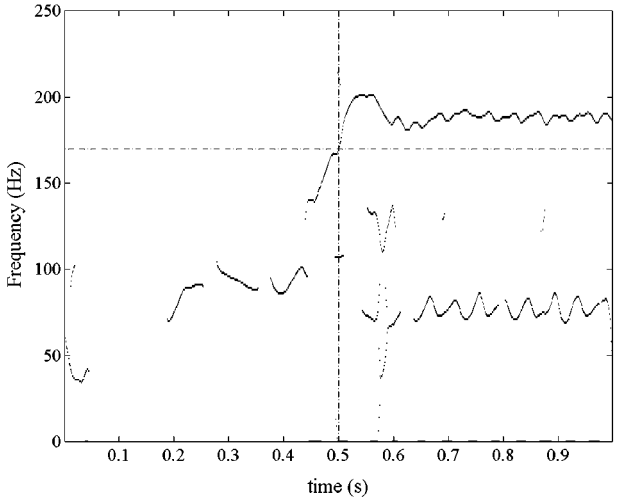

Fig. 11. Ridges of the STFT spectrogram.

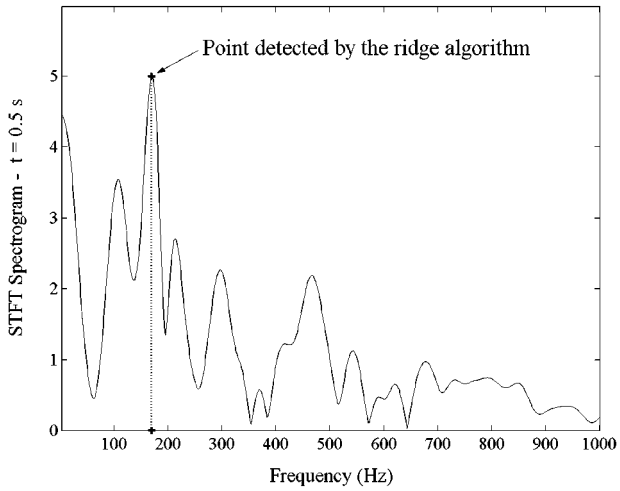

Fig. 12. STFT spectrogram at the instant $t = 0.5$ s.

The corresponding spectrogram $P_W f(u, \xi)$ shown in Fig. 13 is obtained by linearization of the logarithmic scalogram for the AWT, defined by (5)–(13). The scalogram $P_W f(u, s)$ is obtained using six scales, selected as powers of two, $s^{-1} = \{2, 4, 8, 16, 32, 64\}$. An interpolation with 12 voices is also performed. The modulating frequency η and the variance σ are chosen as 5.0 rad/s and 1.0 s, respectively. Darker zones in Fig. 13 also represent high values of the scalogram function in a 3-D plot like the spectrogram in Fig. 10.

Fig. 14 shows the instantaneous frequencies after the use of the ridges algorithm. In this case, less information is lost in the transients and that the resolution is better than that of Fig. 11. Fig. 15 shows the spectrogram at the instant $t = 0.5$ s, and the detected ridge. It is interesting to note that the ridges in Fig. 14 of the AWT near this point ($t = 0.5$ s) have an oscillation not detected by the opto-encoder (Fig. 7, 10 ms between samples) or the STFT, probably because the resolution of the wavelet method is better than the others. In general the AWT algorithm can track fast fluctuations better and can be used for measuring the rotor speed of ac machines.

Faster ridge detection is obtained when the AWT spectrogram is used, because it is a smoother function than the STFT.

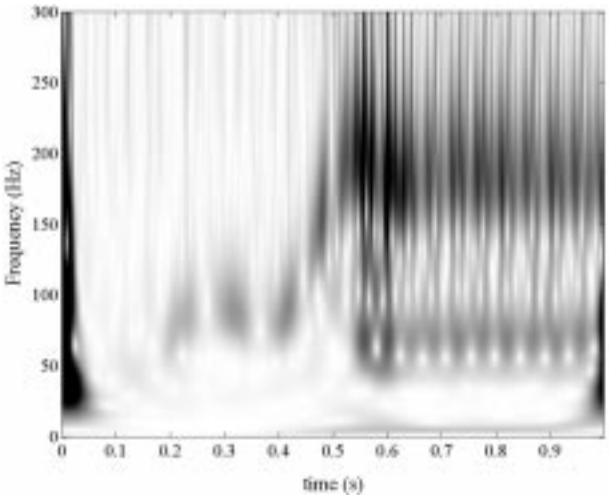

Fig. 13. AWT spectrogram of the stator current.

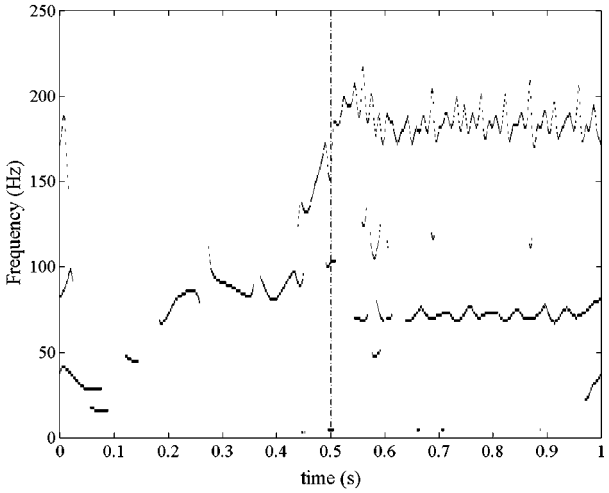

Fig. 14. Ridges of the AWT spectrogram of the stator current.

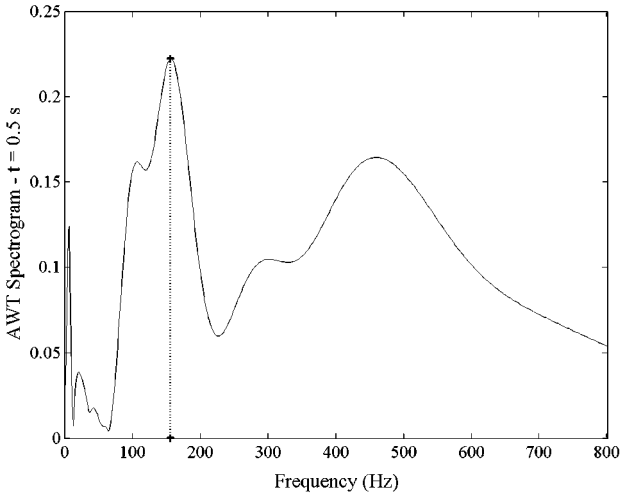

Fig. 15. Detail of the AWT spectrogram for instant $t = 0.5$ s.

Computation time required by AWT is approximately 40% lesser than STFT because the spectrogram is obtained with only six different scales and interpolation of 12 voices per scale (2048×72). The STFT requires 2048 FFT to perform a similar task (2048×2048). All estimations are obtained with offline processing. A conventional FFT algorithm is used to calculate the AWT.

IV. Conclusions

The AWT has been shown to be suitable for measuring the rotor speed of ac machines, during transient or steady-state condition, over the entire speed range. The method can be implemented in real time on a DSP. Compared to the STFT, a better resolution is obtained during transients in the speed with the AWT, even in the low-speed range. The FFT algorithm can be adapted for wavelet transformation or a fast wavelet algorithm can be used to perform the real time calculations. The method can be integrated into DTC drives that use wavelet torque filters with a little increase in computation time. The speed estimation algorithm is almost not affected by the load condition, line voltages or temperature, because time–frequency or time–scale methods depend only on the slot harmonics contained in the phase currents. However, operation in a weakened flux zone can reduce the estimation resolution, because the slot harmonics are also reduced in this case. The ridges algorithm is a simple and powerful way to improve the time–frequency resolution for sensorless speed estimation.

References

[1] P. Vas, *Sensorless Vector and Direct Torque Control*. Oxford, U.K.: Oxford Univ. Press, 1998.

[2] K. D. Hurst and T. G. Habetler, "A comparison of spectrum estimation techniques for sensorless speed detection in induction machines," *IEEE Trans. Ind. Applicat.*, vol. 33, pp. 898–905, July/Aug. 1997.

[3] J. Restrepo and P. Bowler, "Analysis of induction machine slot harmonics in the tf domain," in *Proc. IEEE First Int. Caracas Conf. Devices, Circuits and Systems*, Caracas, Venezuela, 1995, pp. 127–130.

[4] J. A. Restrepo, M. I. Gimenez, V. M. Guzman, J. M. Aller, and A. Bueno, "Kernel selection for sensorless speed measurement of AC machines (Wigner vs. Page representation)," in *Proc. IEEE IECON'98*, vol. 2, Aachen, Germany, 1998, pp. 991–996.

[5] S. Mallat, *A Wavelet Tour of Signal Processing*. New York: Academic, 1999.

[6] N. Delprat, B. Escudié, P. Guillemain, R. Kroland-Martinet, P. Tchamitchian, and B. Torrésani, "Asymptotic wavelet and Gabor analysis: Extraction of instantaneous frequencies," *IEEE Trans. Inform. Theory*, vol. 38, pp. 644–664, Mar. 1992.

[7] M. Depenbrock, "Direct Self-Control (DSC) of inverter-fed induction machine," *IEEE Trans. Power Electron.*, vol. 3, pp. 420–429, Oct. 1988.

[8] T. Naguchi and I. Takahashi, "A new quick-response and high-efficiency control strategy of an induction motor," *IEEE Trans. Ind. Applicat.*, vol. 22, pp. 820–827, Sept./Oct. 1986.

[9] J. Nash, "Direct torque control, induction motor vector control without an encoder," *IEEE Trans. Ind. Applicat.*, vol. 33, pp. 333–341, Mar./Apr. 1997.

[10] J. A. Restrepo, J. M. Aller, T. Pagá, V. M. Guzmán, A. Buen, and M. I. Giménez, "Direct torque control of the induction machine using field oriented method and time frequency transformation for speed estimation and parameter adaptation," in *Proc. ICEM 2000*, vol. 2, Helsinki, Finland, Aug. 2000, pp. 1105–1109.

[11] N. Kasa and H. Watanabe, "A torque ripples compensating technique based on disturbance observer with wavelet transform for sensorless induction motor drive," in *Proc. IEEE IECON'98*, vol. 2, Aachen, Germany, 1998, pp. 580–585.

José M. Aller received the Ing. degree in electrical engineering from Simón Bolívar University, Caracas, Venezuela, in 1980, the M.S. degree in electrical engineering from the Universidad Central de Venezuela, Caracas, Venezuela, in 1982, and the Ph.D. degree in industrial engineering from the Universidad Politécnica de Madrid, Madrid, Spain, in 1993.

For 21 years, he has been a Lecturer at Simón Bolívar University, where he is also currently a full-time Professor in the the Energy Conversion Department. His research interests include space-vector applications, electrical machine control, and power electronics.

Thomas G. Habetler (S'82–M'83–SM'92–F'02) received the B.S.E.E. and M.S. degrees in electrical engineering from Marquette University, Milwaukee, WI, and the Ph.D. degree from the University of Wisconsin, Madison, in 1981, 1984, and 1989, respectively.

From 1983 to 1985, he was a Project Engineer with the Electro-Motive Division, General Motors, where he was involved in the design of switching power supplies and voltage regulators for locomotive applications. He is currently a Professor of Electrical Engineering at Georgia Institute of Technology, Atlanta. His research interests are in switching converter technology and electric machine protection and drives.

Dr. Habetler was corecipient of the 1989 First Prize Paper Award and 1991 Second Prize Paper Award of the Industrial Drives Committee, and 1994 Second Prize Paper Award of the Electric Machines Committee of the IEEE Industry Applications Society (IAS). He serves as the President of the IEEE Power Electronics Society and is Past Chair of the Industrial Power Converter Committee of the IAS.

Ronald G. Harley (M'77–SM'86–F'92) received the M.Sc.Eng. degree in electrical engineering from the University of Pretoria, Pretoria, South Africa, in 1965 and the Ph.D. degree from Imperial College, London, U.K., in 1969.

In 1971, he was appointed Professor of Electric Machines and Control at the University at Natal, Durban, South Africa. He was a Visiting Professor at Iowa State University, Ames, in 1977, Clemson University, Clemson, SC, in 1987, and Georgia Institute of Technology, Atlanta, in 1994. Currently, he is the Duke Power Company Distinguished Professor of Electrical Engineering at Georgia Institute of Technology. His areas of research include power system dynamics, electrical machines, power electronics, and control of ac variable-speed drives.

Dr. Harley is a member of the IEEE Power Engineering and IEEE Industry Applications Societies. He is also a Fellow of the Institution of Electrical Engineers, U.K., and South Africa Institute of Electrical Engineers.

Rangarajan M. Tallam (S'97–M'01) received the B.Tech. degree in electrical engineering from Indian Institute of Technology, Madras, India, in 1997 and the M.S.E.E. and Ph.D. degrees from Georgia Institute of Technology, Atlanta, in 1999 and 2001, respectively.

He is currently a Research Engineer in the Advanced Technology Laboratories, Rockwell Automation, Milwaukee, WI. His research interests are in power converter design and control and condition monitoring of electric machines.

Dr. Tallam was a recipient of Outstanding Doctoral Thesis Awards from the Sigma Xi Honor Society and the School of Electrical and Computer Engineering, Georgia Institute of Technology. He also received the Dr. Ing. Dieter Kind Award for the best undergraduate project in electric power engineering. From 1999 to 2001, he served as the Treasurer and President of the Georgia Institute of Technology Student Chapter of the IEEE Power Engineering Society.

Sang Bin Lee (S'95–M'01) received the B.S. and M.S. degrees in electrical engineering from Korea University, Seoul, Korea, in 1995 and 1997, respectively, and the Ph.D. degree from Georgia Institute of Technology, Atlanta, in 2001.

In 2001, he joined General Electric Corporate Research and Development, Niskayuna, NY, as an Electrical Engineer in the Electromechanical Energy Conversion Laboratory, where he is currently involved in research related to diagnostics and design of electrical machines.